Analytical solutions for transversely isotropic fiber-reinforced composite cylinders under internal or external pressure

İç veya dış basınç altındaki enine izotropik fiber takviyeli kompozit silindirler için analitik çözümler

Yazar(lar) (Author(s)): Ömer Can FARUKOĞLU[1], İhsan KORKUT[2]

ORCID[1]: 0000-0003-3244-8355

ORCID[2]: 0000-0002-5001-4449

Analytical Solutions for Transversely Isotropic Fiber-Reinforced Composite Cylinders under Internal or External Pressure

Highlights

- ❖ *As fiber volume fraction increases, yielding begins at higher strength*
- ❖ *Radial fiber direction gives better results in terms of yielding than axial direction*
- ❖ *Plastic flow takes place at inner radii of the cylinders*

Graphical Abstract

Transversely isotropic fiber reinforced composite cylinders are investigated under internal or external pressure.
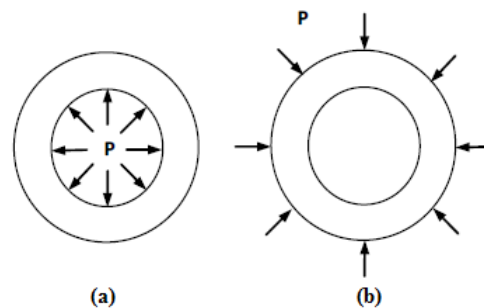

Figure. Cross section of the composite cylinders under **(a)** internal **(b)** external pressure where P denotes pressure

Aim

The aim of this study is examining the elastic stresses of pressurized fiber reinforced composite cylinders which constitute of transversely isotropic fibers and isotropic matrix material.

Design & Methodology

Analytical methods are conducted to analyze stress and displacement field of composite cylinders. In order to calculate composite material properties Chamis method is utilized.

Originality

Analytical solutions are an important tool for better understanding of engineering problems. Solutions that can be a reference for the problem under consideration are obtained.

Findings

Radial fiber alignment, which results in better strength than axial one, is also more complex in terms of analytical approach.

Conclusion

It is observed that fiber volume ratio and fiber direction are important factors affecting elastic limit stress and displacements.

Declaration of Ethical Standards

The authors of this article declare that the materials and methods used in this study do not require ethical committee permission and/or legal-special permission

.

İç veya Dış Basınç Altındaki Enine İzotropik Fiber Takviyeli Kompozit Silindirler için Analitik Çözümler

Ömer Can FARUKOĞLU*, İhsan KORKUT

Department of Manufacturing Engineering, Gazi University, Ankara, Turkey

(Geliş/Received : 26.08.2020 ; Kabul/Accepted : 15.09.2020)

ÖZ

Bu makalede iç veya dış basınç altındaki sabit uçlu kalın cidarlı kompozit silindirlerin elastik gerilmelerini incelemektedir. Silindirler eş yönlü hizalanmış enine izotropik fiber liflerinden ve izotropik matristen meydana gelmektedir. Aksiyel ve radyal fiber yönleri dikkate alınmış ve analitik çözümler buna göre türetilmiştir. Fiber liflerinin yönü ve fiber hacim oranı değişikliğinin elastik gerilmeler üzerindeki etkileri analiz edilmiştir. Hem iç hem de dış basınç durumlarında, fiber yönü ve fiber hacim fraksiyonunun, silindirlerin elastik davranışını etkileyen önemli parametreler olduğu gözlemlenmiştir.

Anahtar Kelimeler: Enine izotropi, kompozit silindirler, elastik gerilmeler, chamis methodu.

Analytical Solutions for Transversely Isotropic Fiber-Reinforced Composite Cylinders under Internal or External Pressure

ABSTRACT

This paper deals with the elastic stresses of internally or externally pressurized long thick-walled composite cylinders with fixed ends. Cylinders are made of unidirectionally aligned transversely isotropic fibers and isotropic matrix. Axial and radial fiber alignments are considered, and analytical solutions are derived accordingly. Effects of fiber direction and fiber volume fraction alteration on the elastic limit stresses are analyzed. It is observed for both internal and external pressure cases that fiber direction and fiber volume fraction are important parameters which impact the elastic behavior of the cylinders.

Keywords: Transverse isotropy, composite cylinders, elastic stresses, chamis method.

1. INTRODUCTION

Prediction of the stresses in axisymmetric geometries such as, disks, shafts and cylinders have been studied by many researchers since such geometries have often been used in engineering fields. Because of the beneficial material properties such as low weight, high strength and corrosion resistance, composites become popular in aerospace and automotive industries. Thus, different parts and components have been produced with composites. According to the enhancements in engineering, first studies on stress analysis are obtained for isotropic thick-walled cylinders subjected to internal and external pressure which can be found in the published books [1, 2]. Stresses of transversely isotropic corrugated cylinders are analyzed by Grigorenko and Rozhok [3]. Another stress analysis research for transversely isotropic cylinders is developed by Sharma et al. [4] where the authors predicted elastic-plastic transition of rotating transversely isotropic cylinders subjected to internal pressure. For functionally graded material cylinders, elastic and/or plastic stress analysis under mechanical [5-10] and thermal [11-13] loads have been the topic of various articles. When it comes to

orthotropic cylinders, studies mainly focus on examining the stresses due to rotation [14–18]. With the developments in material technology, studies have also commenced for cylinders made of fiber reinforced composite materials. Stresses of filament-wound composite cylinders which are subjected to internal pressure and thermal loads are studied by Çallıoğlu et. al. [19]. For multilayered composite cylinders under thermal loads, Akçay and Kaynak [20] proposed analytical solutions. Another stress field study is carried out for laminated composite cylinders subjected to non-axisymmetric loading by Starbuck [21]. Ebeid et. al. [22] predicted the failure of fiber reinforced pipes by using finite element method. In other closely related studies [23,24], composite pressure vessels under different loads, and winding angle optimization of filament wound composite pressure vessels can be found. In the present work, long thick-walled cylinders with closed ends are considered under internal or external pressure. The cylindrical geometry is made of composite material which is composed of transversely isotropic fibers and isotropic matrix. Elastic limit pressure that causes plastic flow in the composite cylinders is calculated by the use of Tsai Wu yield criteria. Axial and radial fiber alignments are taken into account, and analytical approaches are provided for each case. In Figure 1 (a) and

---
*Sorumlu yazar (Corresponding Author)
e-mail : omerfarukoglu08@gmail.com

(b), axial and radial alignment of the fibers in the composite cylinders are displayed where L denotes longitudinal or so-called fiber direction of the composite material, and T is the transverse direction in global coordinates. At Figure 1 (c), lower case l and t presents longitudinal and transverse directions in material coordinates. Additionally, f and m express fibers and matrix respectively.
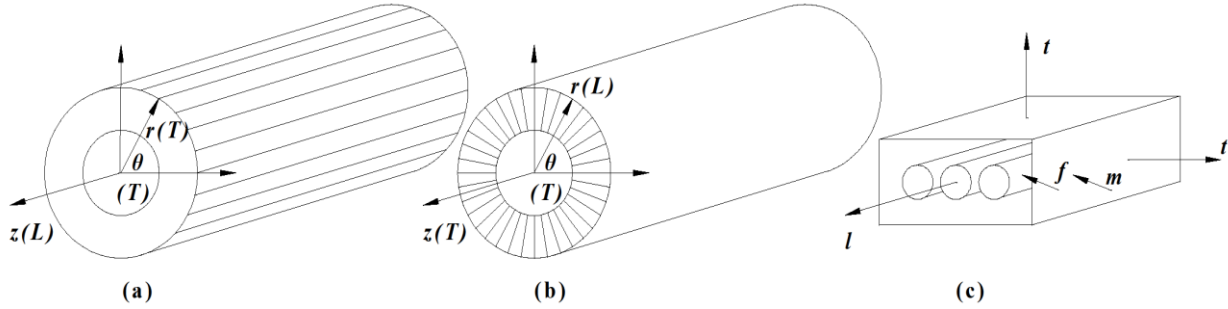
Poisson's ratio of the composite in *T-T* plane is given below.

$$v_{TT} = V_f v_{ttf} + V_m(2v_m - v_{TL}) \qquad (6)$$

in which v_{ttf} is Poisson's ratio of the fibers in *t-t* plane. In order to find elastic limits, it is necessary to define tensile and compressive strength of the composite in both

Figure 1. (a) Axially aligned cylinders **(b)** Radially aligned cylinders **(c)** Unidirectionally aligned fiber reinforced composite

2. CALCULATION OF THE MECHANICAL PROPERTIES

Determination of the mechanical properties of fiber reinforced composites is a long and expensive process since such materials display different properties in various directions. Thus, several models have been developed in the past to calculate the mechanical properties. In this examination, Chamis method [25, 26] is exploited. Fiber volume fraction, mechanical properties of the matrix and fibers are inputs to apply this method. To be noted that in the calculations of the material properties, volume of the voids in the matrix material is not considered.

$$V_f + V_m = 1 \qquad (1)$$

V_f and V_m point to volume fraction of the fibers and matrix. Elastic modulus of the composite material in longitudinal direction (E_L) is calculated by

$$E_L = V_f E_{lf} + V_m E_m \qquad (2)$$

in which E_{lf} and E_m present the elastic modulus of the fibers in longitudinal direction and the elastic modulus of the matrix respectively. Elastic modulus of the composite material in transverse direction (E_T) is

$$E_T = \frac{E_m}{1 - \sqrt{V_f}(1 - \frac{E_m}{E_{tf}})} \qquad (3)$$

where E_{tf} is the elastic modulus of the fibers in transverse direction. In a similar manner, Poisson's ratios of the composite material are determined. Poisson's ratio of the composite in *L-T* plane can be found by

$$v_{LT} = V_f v_{ltf} + V_m v_m \qquad (4)$$

v_{ltf} is the Poisson's ratio of the fibers in *l-t* plane, and v_m denotes the Poisson's ratio of the isotropic matrix. Due to material symmetry, Poisson's ratio of the composite in *T-L* plane is

$$v_{TL} = \frac{E_T}{E_L} v_{LT} \qquad (5)$$

different strength according to the direction.

$$X_t = V_f X_{tf} \qquad (7)$$

$$X_c = V_f X_{cf} \qquad (8)$$

X_t and X_c express tensile and compressive strength of the composite material in longitudinal direction. Similarly, X_{tf} and X_{cf} denote tensile and compressive strength of the fibers in longitudinal direction respectively. Tensile (Y_t) and compressive (Y_c) strength of the composite material in transverse direction are given in Eq.(9) and Eq.(10).

$$Y_t = Y_{tm}[1 - (\sqrt{V_f} - V_f)(1 - \frac{E_m}{E_{tf}})] \qquad (9)$$

$$Y_c = Y_{cm}[1 - (\sqrt{V_f} - V_f)(1 - \frac{E_m}{E_{tf}})] \qquad (10)$$

in which Y_{tm} and Y_{cm} are tensile and compressive strength of the isotropic matrix.

3. ANALYTICAL SOLUTION

It is appropriate to use cylindrical polar coordinate system (r, θ, z). Strain-displacement relation for small axisymmetric deformations can be derived as

$$\varepsilon_r = \frac{du_r(r)}{dr}, \varepsilon_\theta = \frac{u_r(r)}{r}, \varepsilon_z = 0 \qquad (11)$$

u_r, ε_r, ε_θ and ε_z signify radial displacement, radial, tangential and axial elastic strains respectively. Due to the considered fixed ends, axial strain is equal to zero. In order to have an elastic solution, compatibility and equilibrium equations should be satisfied. Regarding compatibility equation is given below.

$$r \frac{d\varepsilon_\theta}{dr} + \varepsilon_\theta - \varepsilon_r = 0 \qquad (12)$$

Equilibrium equation reads as follows

$$\frac{d\sigma_r}{dr} + \frac{1}{r}(\sigma_r - \sigma_\theta) = 0 \qquad (13)$$

in which σ_r and σ_θ are radial and tangential elastic stresses, in addition σ_z denotes the axial elastic stress.

3.1. Axially Aligned Cylinders

In this case, unidirectional fibers in the cylinders are aligned in axial direction, and elastic relations are derived accordingly. By using Hook's law, strain-stress relation is of the form.

$$
\begin{bmatrix} \varepsilon_r \\ \varepsilon_\theta \\ \varepsilon_z \end{bmatrix} = \begin{bmatrix} \frac{1}{E_T} & -\frac{v_{TT}}{E_T} & -\frac{v_{LT}}{E_L} \\ -\frac{v_{TT}}{E_T} & \frac{1}{E_T} & -\frac{v_{LT}}{E_L} \\ -\frac{v_{TL}}{E_T} & -\frac{v_{TL}}{E_T} & \frac{1}{E_L} \end{bmatrix} \begin{bmatrix} \sigma_r \\ \sigma_\theta \\ \sigma_z \end{bmatrix}
\tag{14}
$$

If inverse of the above compliance matrix is taken, we end up with stress-strain relation.

$$
\begin{bmatrix} \sigma_r \\ \sigma_\theta \\ \sigma_z \end{bmatrix} = \begin{bmatrix} \frac{1-v_{LT}v_{TL}}{E_L E_T \Delta} & \frac{v_{TT}+v_{LT}v_{TL}}{E_L E_T \Delta} & \frac{v_{LT}(1+v_{TT})}{E_L E_T \Delta} \\ \frac{v_{TT}+v_{LT}v_{TL}}{E_L E_T \Delta} & \frac{1-v_{LT}v_{TL}}{E_L E_T \Delta} & \frac{v_{LT}(1+v_{TT})}{E_L E_T \Delta} \\ \frac{v_{TL}(1+v_{TT})}{E_T^2 \Delta} & \frac{v_{TL}(1+v_{TT})}{E_T^2 \Delta} & \frac{1-v_{TT}^2}{E_T^2 \Delta} \end{bmatrix} \begin{bmatrix} \varepsilon_r \\ \varepsilon_\theta \\ \varepsilon_z \end{bmatrix},
$$

$$
\Delta = \frac{(1+v_{TT})(1-v_{TT}-2v_{LT}v_{TL})}{E_L E_T^2}
\tag{15}
$$

For the axially aligned fibers, stress-strain relation is described with the above stiffness matrix. It should be noted that both compliance and stiffness matrices are symmetric. Since all elastic relations are defined, compatibility and equilibrium equations given in Eq.(12) and Eq.(13) can be solved. By substituting strain terms given in Eq.(11) into Eq.(12), compatibility condition gets satisfied. In order to solve the equilibrium equation, firstly, elastic strains in Eq.(11) should be substituted to Eq.(15). Subsequently, directional stresses given in Eq.(15) are substituted into Eq.(13). After several algebraic operations we arrive at the below homogeneous Cauchy-Euler differential equation.

$$
r^2 \frac{du_r^2}{dr^2} + r \frac{u_r}{dr} - u_r = 0
\tag{16}
$$

General solution of Eq.(16) is

$$
u_r(r) = \frac{C_1}{r} + C_2 r
\tag{17}
$$

in which C_1 and C_2 are arbitrary constants to be determined according to the boundary conditions. Since the general solution of the radial displacement is acquired at Eq.(17), radial and tangential strains can be found by applying Eq.(11) to Eq.(17).

$$
\varepsilon_r(r) = -\frac{C_1}{r^2} + C_2
\tag{18}
$$

$$
\varepsilon_\theta(r) = \frac{C_1}{r^2} + C_2
\tag{19}
$$

If Eq.(18) and Eq.(19) are substituted to Eq.(15), directional stresses can be achieved.

$$
\sigma_r(r) = -C_1 \frac{E_T}{1+v_{TT}} r^{-2} + C_2 \frac{E_T}{1-v_{TT}-2v_{LT}v_{TL}}
\tag{20}
$$

$$
\sigma_\theta(r) = C_1 \frac{E_T}{1+v_{TT}} r^{-2} + C_2 \frac{E_T}{1-v_{TT}-2v_{LT}v_{TL}}
\tag{21}
$$

$$
\sigma_z(r) = C_2 \frac{2E_L v_{TL}}{1-v_{TT}-2v_{LT}v_{TL}}
\tag{22}
$$

For the axially aligned cylinders, which are subjected to internal pressure, C_1 and C_2 are attained by using the following boundary conditions.

$$
\sigma_r(a) = -P_{in}, \ \sigma_r(b) = 0
\tag{23}
$$

where a and b denote the inner and outer radius of the cylinders, and P_{in} is the elastic limit internal pressure. If the conditions given in Eq.(23) are solved with Eq.(20), arbitrary constants can be established.

$$
C_1 = -\frac{a^2 b^2 P_{in}(1+v_{TT})}{E_T(a^2-b^2)}
\tag{24}
$$

$$
C_2 = -\frac{a^2 P_{in}(1-v_{TT}-2v_{LT}v_{TL})}{E_T(a^2-b^2)}
\tag{25}
$$

Similarly, when the axially aligned cylinders are under external pressure, boundary conditions take the below form.

$$
\sigma_r(a) = 0, \ \sigma_r(b) = -P_{ex}
\tag{26}
$$

in which P_{ex} is the elastic limit external pressure. C_1 and C_2 can be found by applying Eq.(26) to Eq.(20).

$$
C_1 = \frac{a^2 b^2 P_{ex}(1+v_{TT})}{E_T(a^2-b^2)}
\tag{27}
$$

$$
C_2 = \frac{b^2 P_{ex}(1-v_{TT}-2v_{LT}v_{TL})}{E_T(a^2-b^2)}
\tag{28}
$$

Since the cylindrical geometry has fixed ends, stress occurs at the axial direction. Accordingly, axial force is calculated with the following integration.

$$
F_z = \int_a^b 2\pi r \sigma_z dr
\tag{29}
$$

3.2. Radially Aligned Cylinders

In this section, transversely isotropic fibers are unidirectionally aligned in radial direction, and analytical derivations are obtained in this regard. Basic relations given in Eqs.(11)-(13) remains the same. On the other hand, when fiber direction is altered to radial direction, strain-stress relation becomes

$$
\begin{bmatrix} \varepsilon_r \\ \varepsilon_\theta \\ \varepsilon_z \end{bmatrix} = \begin{bmatrix} \frac{1}{E_L} & -\frac{v_{TL}}{E_T} & -\frac{v_{TL}}{E_T} \\ -\frac{v_{LT}}{E_L} & \frac{1}{E_T} & -\frac{v_{TT}}{E_T} \\ -\frac{v_{LT}}{E_L} & -\frac{v_{TT}}{E_T} & \frac{1}{E_T} \end{bmatrix} \begin{bmatrix} \sigma_r \\ \sigma_\theta \\ \sigma_z \end{bmatrix}
\tag{30}
$$

Stress-strain relation take the below form after fiber alignment is shifted

$$
\begin{bmatrix} \sigma_r \\ \sigma_\theta \\ \sigma_z \end{bmatrix} = \begin{bmatrix} \frac{1-v_{TT}^2}{E_T^2 \Delta} & \frac{v_{TL}(1+v_{TT})}{E_T^2 \Delta} & \frac{v_{TL}(1+v_{TT})}{E_T^2 \Delta} \\ \frac{v_{LT}(1+v_{TT})}{E_L E_T \Delta} & \frac{1-v_{LT}v_{TL}}{E_L E_T \Delta} & \frac{v_{TT}+v_{LT}v_{TL}}{E_L E_T \Delta} \\ \frac{v_{LT}(1+v_{TT})}{E_L E_T \Delta} & \frac{v_{TT}+v_{LT}v_{TL}}{E_L E_T \Delta} & \frac{1-v_{LT}v_{TL}}{E_L E_T \Delta} \end{bmatrix} \begin{bmatrix} \varepsilon_r \\ \varepsilon_\theta \\ \varepsilon_z \end{bmatrix}
\tag{31}
$$

In the above equation, Δ given in Eq.(15) remains the same. In order to satisfy the equilibrium equation, Eq.(11) is substituted to Eq.(31). Followingly, corresponding stresses in Eq.(31) are substituted to Eq.(13). Once again homogeneous Cauchy-Euler type differential equation is acquired.

$$r^2 \frac{du_r^2}{dr^2} + r\frac{u_r}{dr} - \frac{s_{22}}{s_{11}}u_r = 0 \tag{32}$$

in which s_{11} and s_{22} are the stiffness matrix terms of Eq.(31). By solving the above differential equation, general solution of the radial displacement is achieved.

$$u_r(r) = C_1 r^{-\lambda} + C_2 r^\lambda, \quad \lambda = \sqrt{\frac{s_{22}}{s_{11}}} = \sqrt{\frac{E_T(1-\nu_{LT}\nu_{TL})}{E_L(1-\nu_{TT}^2)}} \tag{33}$$

Implementing Eq.(11) to Eq.(33), radial and tangential strains are found.

$$\varepsilon_r(r) = C_1 \lambda r^{-\lambda-1} + C_2 \lambda r^{\lambda-1} \tag{34}$$

$$\varepsilon_\theta(r) = C_1 r^{-\lambda-1} + C_2 r^{\lambda-1} \tag{35}$$

Directional stresses are obtained via substituting Eq.(34) and Eq.(35) to Eq.(31).

$$\sigma_r(r) = C_1 \frac{E_L(\nu_{TL}+\lambda(\nu_{TT}-1))}{1-\nu_{TT}-2\nu_{LT}\nu_{TL}} r^{-\lambda-1} + C_2 \frac{E_L(\nu_{TL}-\lambda(\nu_{TT}-1))}{1-\nu_{TT}-2\nu_{LT}\nu_{TL}} r^{\lambda-1} \tag{36}$$

$$\sigma_\theta(r) = C_1 \frac{E_T(1-\nu_{LT}(\lambda(\nu_{TT}+1)+\nu_{TL}))}{(1-\nu_{TT}-2\nu_{LT}\nu_{TL})(\nu_{TT}+1)} r^{-\lambda-1} + C_2 \frac{E_T(1+\nu_{LT}(\lambda(\nu_{TT}+1)-\nu_{TL}))}{(1-\nu_{TT}-2\nu_{LT}\nu_{TL})(\nu_{TT}+1)} r^{\lambda-1} \tag{37}$$

$$\sigma_z(r) = C_1 \frac{E_T(\nu_{TT}+\nu_{LT}(\nu_{TL}-\lambda(\nu_{TT}+1)))}{(1-\nu_{TT}-2\nu_{LT}\nu_{TL})(\nu_{TT}+1)} r^{-\lambda-1} + C_2 \frac{E_T(\nu_{TT}+\nu_{LT}(\nu_{TL}+\lambda(\nu_{TT}+1)))}{(1-\nu_{TT}-2\nu_{LT}\nu_{TL})(\nu_{TT}+1)} r^{\lambda-1} \tag{38}$$

When the radially aligned cylinders are subjected to internal pressure, arbitrary constants are attained by applying Eq.(36) to Eq.(23).

$$C_1 = \frac{a^{\lambda+1}b^{2\lambda}P_{in}(1-\nu_{TT}-2\nu_{LT}\nu_{TL})}{E_L(a^{2\lambda}-b^{2\lambda})(\nu_{TL}+\lambda(\nu_{TT}-1))} \tag{39}$$

$$C_2 = -\frac{a^{\lambda+1}P_{in}(1-\nu_{TT}-2\nu_{LT}\nu_{TL})}{E_L(a^{2\lambda}-b^{2\lambda})(\nu_{TL}-\lambda(\nu_{TT}-1))} \tag{40}$$

In a similar manner, for the externally pressurized composite cylinders, which constitutes of radially aligned fibers, C_1 and C_2 are achieved with using Eq.(36) and Eq.(26).

$$C_1 = -\frac{a^{2\lambda}b^{\lambda+1}P_{ex}(1-\nu_{TT}-2\nu_{LT}\nu_{TL})}{E_L(a^{2\lambda}-b^{2\lambda})(\nu_{TL}+\lambda(\nu_{TT}-1))} \tag{41}$$

$$C_2 = \frac{b^{\lambda+1}P_{ex}(1-\nu_{TT}-2\nu_{LT}\nu_{TL})}{E_L(a^{2\lambda}-b^{2\lambda})(\nu_{TL}-\lambda(\nu_{TT}-1))} \tag{42}$$

3.3. Elastic Limits

In order to find the elastic limits, Tsai-Wu yield criteria [27] is utilized. Corresponding criteria in principal directions is given below.

$$\sigma_Y(r) = F_1\sigma_r + F_2\sigma_\theta + F_3\sigma_z + F_{11}\sigma_r^2 + F_{22}\sigma_\theta^2 + F_{33}\sigma_z^2 + 2F_{12}\sigma_r\sigma_\theta + 2F_{13}\sigma_r\sigma_z + 2F_{23}\sigma_\theta\sigma_z \le 1 \tag{43}$$

in which F_j and F_{ij} terms are the coefficients of the yielding criteria, which are calculated by using tensile and compressive strengths of the composite material stated in Eq.(7) to Eq.(10). When the fibers are taken in axial direction, coefficients become

$$F_1 = F_2 = \frac{1}{Y_t} - \frac{1}{Y_c}, \quad F_3 = \frac{1}{X_t} - \frac{1}{X_c},$$

$$F_{11} = F_{22} = \frac{1}{Y_tY_c}, \quad F_{33} = \frac{1}{X_tX_c},$$

$$F_{12} = \frac{-1}{2\sqrt{Y_tY_cY_tY_c}}, \quad F_{13} = F_{23} = \frac{-1}{2\sqrt{X_tX_cY_tY_c}} \tag{44}$$

In the case of radial fiber alignment, F_j and F_{ij} terms take the below forms

$$F_1 = \frac{1}{X_t} - \frac{1}{X_c}, \quad F_2 = F_3 = \frac{1}{Y_t} - \frac{1}{Y_c},$$

$$F_{11} = \frac{1}{X_tX_c}, \quad F_{22} = F_{33} = \frac{1}{Y_tY_c},$$

$$F_{12} = F_{13} = \frac{-1}{2\sqrt{X_tX_cY_tY_c}}, \quad F_{23} = \frac{-1}{2\sqrt{Y_tY_cY_tY_c}} \tag{45}$$

Since this study focuses on the elastic stresses, Eq.(43) should not exceed 1. As long as Eq.(43) is smaller than 1, all elastic relations are valid. In this regard, elastic limit internal or external pressure values are calculated when Eq.(43) is equal to 1. Plastic flow commences when $\sigma_Y(r) > 1$.

4. NUMERICAL RESULTS

In order to display numerical examples, geometric properties of the cylinders and mechanical properties of the composite material should be determined. In this regard, inner (a) and outer (b) radii of the cylinders are taken as 0.05 m and 0.10 m respectively. Graphite/epoxy is utilized as the material of the cylinders. Mechanical properties of transversely isotropic graphite fibers and isotropic epoxy are given in Table 1. Composite material properties are calculated by employing Chamis method from Eq.(1) to Eq.(10) with the data given in Table 1. Followingly, variables are converted to their non-dimensional forms to exemplify numerical results more conveniently. Normalized variables are exhibited with overbars. Correspondingly, radial coordinate of the cylinders become $\bar{r} = r/b$. Directional and yield stresses are $\bar{\sigma}_j = \sigma_j/Y_{cm}, \bar{\sigma}_Y(r) = \sigma_Y(r)$. As it is seen yield stress does not require normalization because Eq.(43) is already in dimensionless form. Elastic limit pressures take the following form $\bar{P}_{in} = P_{in}/Y_{cm}$ and $\bar{P}_{ex} = P_{ex}/Y_{cm}$. Normalized radial displacement is $\bar{u}_r = u_rE_m/Y_{cm}b$. Axial force becomes $\bar{F}_z = F_zb/Y_{cm}$. When fibers are axially aligned, arbitrary constants are $\bar{C}_1 = C_1/b^2$ and $\bar{C}_2 = C_2$. On the other hand, when the fibers are taken radially $\bar{C}_1 = C_1/b^{1+\lambda}$ and $\bar{C}_2 = C_2/b^{1-\lambda}$. It should be noted that in the following numerical examples all directional stresses, radial displacements, radial coordinates and regarding variables are exhibited in dimensionless forms.

Table 1. Micromechanical properties of the graphite fibers and epoxy [28]

E_{lf} (GPa)	E_{tf} (GPa)	E_m (GPa)	ν_{ltf} (-)	ν_{ttf} (-)	ν_m (-)	X_{tf} (MPa)	X_{cf} (MPa)	Y_{tm} (MPa)	Y_{cm} (MPa)
230	22	3.4	0.30	0.35	0.30	2067	1999	72	102

4.1. Axially Aligned Cylinders Under Internal Pressure

In this case, equations given from (17) to (22) are valid, and the boundary conditions presented in Eq.(24) and Eq.(25) are used. Axial force is found by using the integration given in Eq.(29), and the elastic limit internal pressure values are obtained by using Tsai-Wu yield criteria with the conditions in Eq.(44). For various composite material compositions, which are calculated with altering the V_f values, obtained non dimensional results are exhibited below.

Table 2. Dimensionless results of the axially aligned composite cylinders subjected to internal pressure for different V_f

	V_f=0.25	V_f=0.50	V_f=0.75
$\bar{C}_1$	0.002367	0.001665	0.001164
$\bar{C}_2$	0.000729	0.000594	0.000480
$\bar{F}_z$	0.012750	0.013326	0.014566
$\bar{P}_{in}$	0.270573	0.282793	0.309180

It is displayed in Table 2 that when fiber volume fraction increases, cylinders begin yielding at higher internal pressure values which can be seen by tracking $\bar{P}_{in}$. In addition, when the applied maximum elastic pressure increase, axial force ($\bar{F}_z$) at the fixed-ends of the cylinders also rise. Followingly, corresponding stress and radial displacement fields are illustrated graphically. In Figure 2 (a) (b) and (c), when V_f enlarges directional stresses in all directions ascend. Axial stress is considerably small when it is compared to radial and tangential stresses, and it does not vary through radius which is in compliance with the analytical derivation given in Eq.(22). Another aspect is that, under internal pressure, tangential and axial stresses are tensile, however, radial stress is compressive. It is spotted from Figure 2 (d) that plastic flow commences at the inner radii of the cylinders. In addition, cylinders radially expand when internally pressurized, and as the value of V_f rises radial displacement descends which is depicted by Fig. 2 (e). Composite material gets stiffer as the fiber volume fraction rises. Thus, the radial displacement reduces.
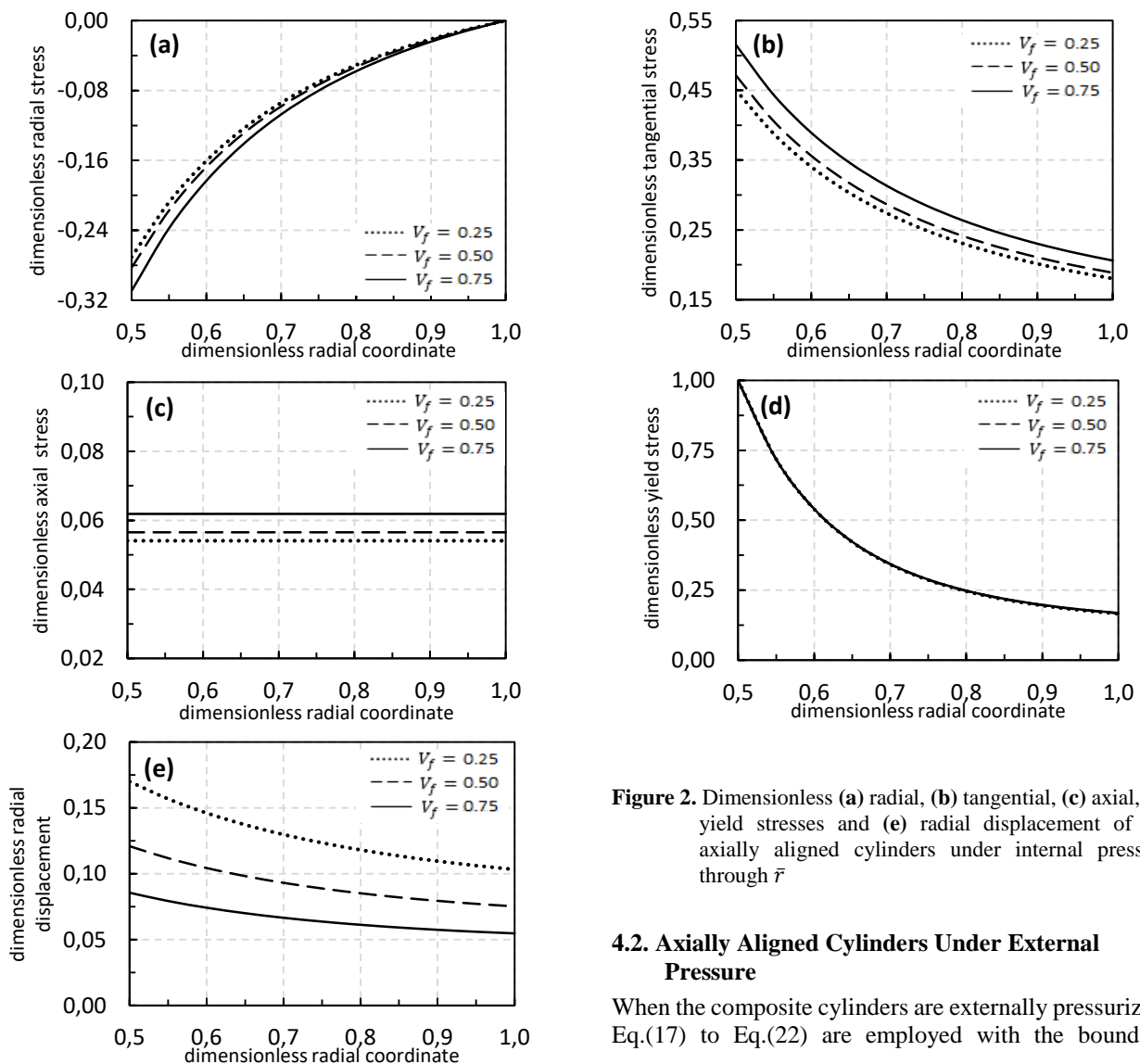

Figure 2. Dimensionless **(a)** radial, **(b)** tangential, **(c)** axial, **(d)** yield stresses and **(e)** radial displacement of the axially aligned cylinders under internal pressure through $\bar{r}$

### 4.2. Axially Aligned Cylinders Under External Pressure

When the composite cylinders are externally pressurized, Eq.(17) to Eq.(22) are employed with the boundary

conditions in Eq.(27) and Eq.(28). Calculated results for these conditions are presented below.

Table 3. Dimensionless results of the axially aligned composite cylinders subjected to external pressure for different V_f

	V_f=0.25	V_f=0.50	V_f=0.75
$\bar{C}_1$	-0.002645	-0.001843	-0.001285
$\bar{C}_2$	-0.003260	-0.002632	-0.002118
$\bar{F}_z$	-0.057000	-0.058998	-0.064302
$\bar{P}_{ex}$	0.302395	0.312998	0.341136

According to the obtained results in Table 3, as expected, strength of the cylinders enhances with the increase of V_f
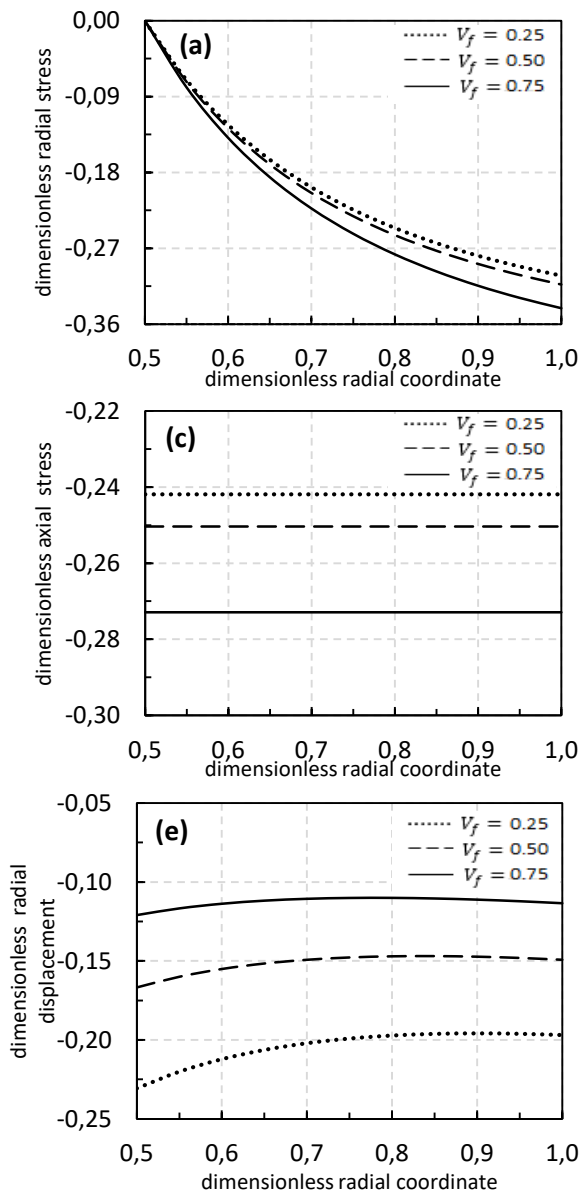
external pressure, axial force is compressive. Incrementing V_f cause enlargement to axial force at the ends of the cylinders. All the normalized directional stresses are compressive under external pressure. Once again, axial stress does not alter with the radii of the cylinders as in the previously illustrated internal pressure case. Figure 3 (d) presents that even though the cylinders are externally pressurized yielding begins at $r = a$. This situation is explained by the fact that directional stress difference is maximum at the inner diameter of cylinders. Additionally, directional stresses expand with the increase of fiber volume fraction. In this boundary condition, composite cylinders shrink in radial direction which is plotted at Fig 3 (e). This shrinkage is the highest at the inner radii of the cylinders since yielding begins there.
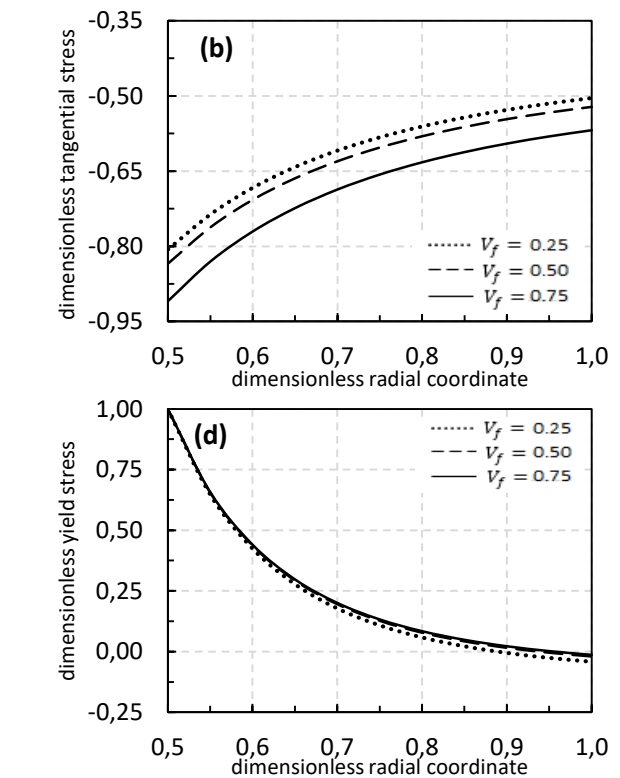
Figure 3. Dimensionless **(a)** radial, **(b)** tangential, **(c)** axial, **(d)** yield stresses and **(e)** radial displacement of the axially aligned cylinders under external pressure through $\bar{r}$

4.3. Radially Aligned Cylinders Under Internal Pressure

Eq.(33) to Eq.(38) are applied for the radially aligned composite cylinders subjected to internal pressure, and arbitrary constants given in Eq.(39) and Eq.(40) are used. Axial force at the fixed-ends are calculated by employing Eq.(38) to Eq.(29) with the corresponding boundary conditions. Additionally, $\bar{P}_{in}$ is found by utilizing Eq.(43) with Eq.(45). Under these terms, acquired outcomes are demonstrated at Table 4.

which is observed by comparing elastic limit external pressure values. Moreover, In Table 3, dimensionless axial force terms have negative sign in front which indicates that when composite cylinders are under

Table 4. Dimensionless results of the radially aligned composite cylinders subjected to internal pressure for different V_f

	V_f=0.25	V_f=0.50	V_f=0.75
$\bar{C}_1$	0.001914	0.001520	0.001188
$\bar{C}_2$	0.001366	0.001161	0.000923
$\bar{F}_z$	0.041410	0.040954	0.039864
$\bar{P}_{in}$	0.361459	0.395519	0.439980

radially aligned cylinders are similar to each other, but radial fiber alignment creates higher elastic stresses. On the other hand, axial stress of the axially (Fig 2 (c)) and radially (Fig 4 (c)) aligned cylinders exhibit difference. The reason of this difference is observed by comparing Eq.(22) and Eq.(38). Eq.(22) is independent of the radial coordinate, however Eq.(38) is a function of r, and much sophisticated due to λ term. When the radial displacements of the axially (Fig 2 (e)) and radially (Fig 4 (e)) aligned cylinders under internal pressure are

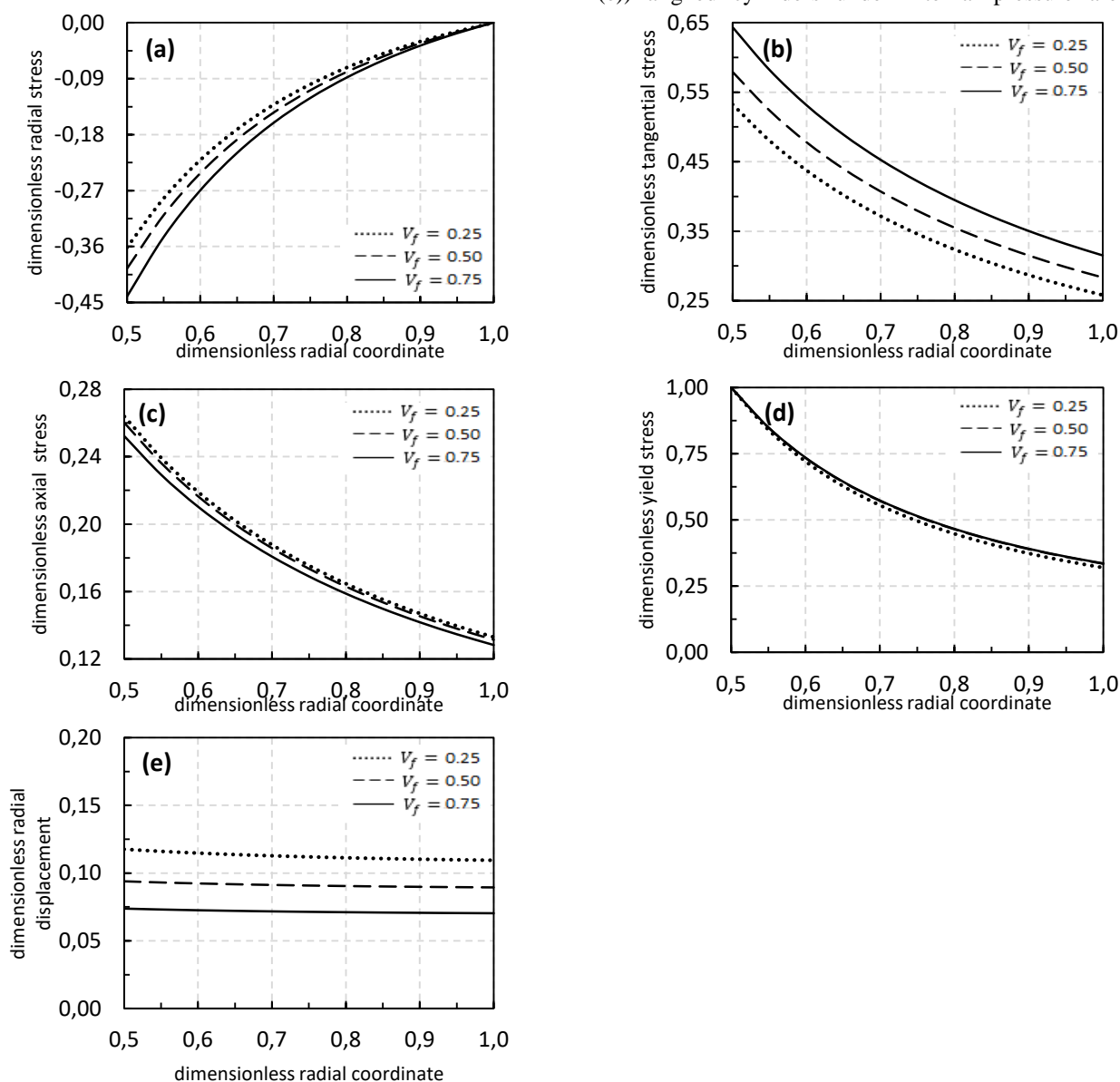**Figure 4.** Dimensionless **(a)** radial, **(b)** tangential, **(c)** axial, **(d)** yield stresses and **(e)** radial displacement of the radially aligned cylinders under internal pressure through $\bar{r}$

When fiber direction is switched from axial to radial, composite cylinders begin yielding at greater elastic limit internal pressure values which is understood by checking $\bar{P}_{in}$ in Table 2 and Table 4. By comparing Fig 2 (a)-(b) with Fig 4 (a)-(b), one can comprehend that radial and tangential stress distribution profiles of the axially and

compared, it is noticed that displacement profiles moderately alter especially at $r = a$. The cause of this alteration is found with monitoring Eq.(17) and Eq.(33). The term λ in Eq.(33) influences the displacement of the radially aligned cylinders.

4.4. Radially Aligned Cylinders Under External Pressure

In this final case, boundary conditions stated in Eq.(41) and Eq.(42) are operated from Eq.(33) to Eq.(38). Achieved results for various V_f are presented at the following table and figures.

Table 5. Dimensionless results of the radially aligned composite cylinders subjected to external pressure for different V_f

	V_f=0.25	V_f=0.50	V_f=0.75
$\bar{C}_1$	-0.002981	-0.002328	-0.001767
$\bar{C}_2$	-0.003525	-0.002705	-0.002068
$\bar{F}_z$	-0.086645	-0.080117	-0.075670
$\bar{P}_{ex}$	0.362273	0.373638	0.401372

s noticed from Table 5, $\bar{P}_{ex}$ increases with higher V_f, and $\bar{F}_z$ is compressive which is in compliance with the case given in section 4.2. When the cylinders are externally pressurized, radially aligned cylinders start yielding at higher $\bar{P}_{ex}$ values than the axially aligned ones. This comparison is validated by checking the results in Table 3 and Table 5. Radial and tangential elastic stress distributions of the axially (Fig 3 (a)-(b)) and radially (Fig 5 (a)-(b)) aligned cylinders are similar. On the other hand, these radial and tangential stresses are moderately higher when fibers are radially aligned. Conversely, axial stresses of the axially (Fig 3 (c)) and radially (Fig 5 (c)) aligned cylinders deviate from each other. When Fig 3 (e) and Fig 5 (e) are cross checked, it is acquired that displacements of the externally pressurized cylinders relatively vary at $r = b$. This change is, once again, resulted by the term λ.
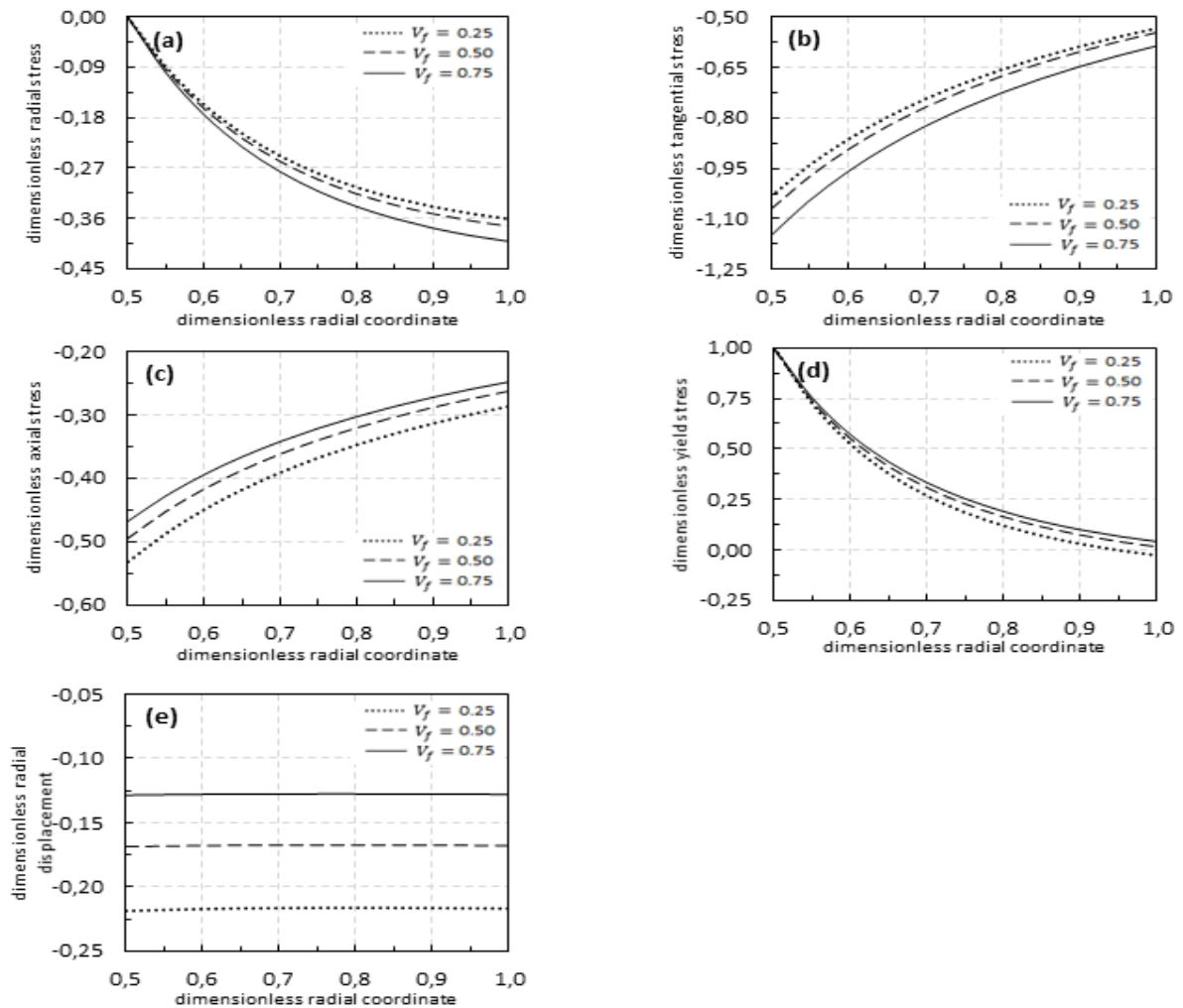

Figure 5. Dimensionless **(a)** radial, **(b)** tangential, **(c)** axial, **(d)** yield stresses and **(e)** radial displacement of the radially aligned cylinders under external pressure through $\bar{r}$

5. CONCLUDING REMARKS

The aim of this study is investigating the elastic limit stress and displacement field of long thick-walled fiber reinforced composite cylinders in the framework of elasticity. In this regard, analytical derivations are obtained for cylinders which have unidirectionally aligned fibers in axial and radial directions, and solutions are presented for internal and external pressure cases. In order to find the elastic limits Tsai-Wu yield criteria is employed. Throughout the applied cases, yielding takes place at the inner surface of the cylinders because of the directional stress difference which is at apex point in $r = a$. On the other hand, it is hard to make a statement as transversely isotropic fibers always fail at the inner radius. For different composite material properties, fiber alignments, wall thicknesses, or different failure criteria, these structures may start yielding elsewhere. As expected, values of the composite material properties rise with the increment of V_f. Therefore, the higher V_f is the higher elastic limit internal or external pressure values become. Another important point that should be mentioned is when fiber direction is taken radially, cylinders start yielding at the higher elastic limits. Thus, if axial and radial fiber alignment are compared, radial direction would be the preferred direction for better performance.

DECLARATION OF ETHICAL STANDARDS

The authors of this article declare that the materials and methods used in this study do not require ethical committee permission and/or legal-special permission.

AUTHORS' CONTRIBUTIONS

Ömer Can FARUKOĞLU: Modeling, analyzing and writing.

İhsan KORKUT: Supervising and editing.

CONFLICT OF INTEREST

There is no conflict of interest in this study.

REFERENCES

[1] Ugural A. C., and Fenster S. K., "Advanced Mechanics of Materials and Applied Elasticity", *Prentice Hall*, New Jersey, (2003).

[2] Timoshenko S. P., and Goodier J. N., "Theory of Elasticity", *McGraw Hill*, Palo Alto, (1951).

[3] Grigorenko Y. M., and Rozhok L.S., "Stress solutions for transversely isotropic corrugated hollow cylinders. International Applied Mechanics", *International Applied Mechanics*, 41(3): 277-282, (2005).

[4] Sharma S., Sahni M., and Kumar R., "Elastic-plastic transition of transversely isotropic thick-walled rotating cylinder under internal pressure", *Defense Science Journal*, 59(3): 260-264, (2009).

[5] Chen Y. Z., and Lin X. Y., "Elastic analysis for thick cylinders and spherical pressure vessels made of functionally graded materials", *Computational Materials Science*, 44(2): 581-587, (2008).

[6] Fukui Y., and Yamanaka N., "Elastic analysis for thick-walled tubes of functionally graded material subjected to internal pressure", *JSME International Journal. Ser.1, Solid Mechanics, Strength of Materials*, 35(4): 379-385, (1992).

[7] Dui G., Xin L.,Yang S., and Zhang J., "An elasticity solution for functionally graded thick-walled tube subjected to internal pressure", *International Journal of Mechanical Sciences*, 89: 344–349, (2014).

[8] Eraslan A. N., and Akış T., "Plane strain analytical solutions for a functionally graded elastic–plastic pressurized tube", *International Journal of Pressure Vessels and Piping*, 83: 635–644, (2006).

[9] Tütüncü N., "Stresses in thick-walled fgm cylinders with exponentially-varying properties", *Engineering Structures*, 29: 2032–2035, (2007).

[10] Akış T., and Eren Ö., "Radyal Yönde Basınç Uygulanan Fonksiyonel Derecelendirilmiş Malzemeden Yapılmış Uzun Tüplerde Von Mises Kriterine Göre Akmanın Başlaması", *Politeknik Dergisi*, 18(2): 63-71, (2015).

[11] Asgari M., and Akhlaghi M., "Transient thermal stresses in two-dimensional functionally graded thick hollow cylinder with finite length", *Archive of Applied Mechanics*, 80: 353-376, (2010).

[12] Shao Z. S., "Mechanical and thermal stresses of a functionally graded circular hollow cylinder with finite length", *International Journal of Pressure Vessels and Piping*, 82: 155–163, (2005).

[13] Ohmichi M., and Noda N., "Steady thermal stresses in functionally graded eccentric polygonal cylinder with circular hole", *Archive of Applied Mechanics*, 86: 1163–1177, (2016).

[14] Leu S. Y., and Hsu H. C., "Exact solutions for plastic responses of orthotropic strain-hardening rotating hollow cylinders", *International Journal of Mechanical Sciences*, 52: 1579–1587 (2010).

[15] Tervonen M., and Pramila A., "Stress in a hollow rotating cylindrically orthotropic tube", *Mechanics of Composite Materials*, 32(6): 577-581, (1996).

[16] Abd-Alla A. M., Mahmoud S. R., and AL-Shehri N. A., "Effect of the rotation on a non-homogeneous infinite cylinder of orthotropic material", *Applied Mathematics and Computation*, 217: 8914–8922, (2011).

[17] Garmestani H., Vaghar M. R., Markiewicz D., and Chandra, N., "Stress analysis of an orthotropic work-hardening cylinder with body force", *Journal of Structural Mechanics*, 23(4): 521-548, (1995).

[18] Zenkour A. M., "Rotating variable-thickness orthotropic cylinder containing a solid core of uniform-thickness", *Archive of Applied Mechanics*, 76: 89–102, (2006).

[19] Çallıoğlu H., Ergün E., and Demirdağ O., "Stress analysis of filament-wound composite cylinders under combined internal pressure and thermal loading", *Advanced Composites Letters*, 17(1): 13-21, (2008).

[20] Akcay I. H., and Kaynak I., "Analysis of multilayered composite cylinders under thermal loading", *Journal of Reinforced Plastics and Composites*, 24(11): 1169-1179, (2005).

[21] Starbuck J. M., "Stress analysis of laminated composite cylinders under non-axisymmetric loading*", Oak Ridge National Laboratory (ORNL)*, Oak Ridge, TN, (1999).

[22] Ebeid S., Taha I., and Abdel-Ghany A. W., "Failure prediction of fiber reinforced polymer pipes using fea", *International Journal of Engineering and Technical Research*, 4(2): 2454-4698, (2016).

[23] Parnas L., and Katırcı N., "Design of fiber-reinforced composite pressure vessels under various loading conditions", *Composite Structures*, 58(1): 83-95, (2002).

[24] Geng P., Xing J. Z., and Chen X. X., "Winding angle optimization of filament-wound cylindrical vessel under internal pressure", *Archive of Applied Mechanics*, 87(3): 365-384, (2017).

[25] Chamis C. C., "Mechanics of composite materials: past, present, and future", *Journal of Composites, Technology and Research*, 11(1): 3-14, (1989).

[26] Chamis C. C., "Simplified Composite Micromechanics Equations for Strength, Fracture Toughness, Impact Resistance and Environmental Effects", *National Aeronautics and Space Administration (NASA)*, CL. OH., (1984).

[27] Tsai S. W., and Wu E. M., "A general theory of strength for anisotropic materials*", Journal of Composite Materials*, 5(1): 58-80, (1971).

[28] Kaw A. K., "Mechanics of Composite Materials", *CRC Press*, Boca Raton, (2006).